Nanoscale

RSC Publishing

PAPER

The optoelectronic behaviour of carbon nanoparticles: evidence of the importance of the outer carbon shell†

Cite this: *Nanoscale*, 2013, **5**, 7977

Gabriela Marzari,[a] Gustavo M. Morales,*[a] M. Sergio Moreno,[b] D. I. Garcia-Gutierrez[c] and Fernando Fungo*[a]

Received 25th March 2013
Accepted 20th June 2013

DOI: 10.1039/c3nr01485a

www.rsc.org/nanoscale

The particular properties of carbon nanoparticles (CNPs) have generated great interest in biomedicine, bioanalysis and optoelectronics. However, an association between the CNPs' physicochemical properties with their molecular and morphological characteristics is, even today, a topic of discussion. In this work, we use a simple method of synthesis with the ultimate aim of elucidating the structural nature of the obtained CNPs and its relationship with their well-known fluorescent properties. The sample is studied by high-resolution transmission electron microscopy (HRTEM), electron energy-loss spectroscopy (EELS), nuclear magnetic resonance (NMR), UV-visible and IR spectroscopy, electrochemistry and electrogenerated chemiluminescence (ECL). The results showed that the nanoparticles are constituted by a graphitic core surrounded by an amorphous layer, which seems to be significant in the determination of the optical and electronic properties observed in the system under study.

1 Introduction

Carbon nanoparticles (CNPs) are among the latest discovered nanoparticles of a single element. Xu *et al.* in 2004 reported the finding of fluorescent carbon particles as impurities of a single-walled carbon nanotube synthesis.[1] Since then, there has been an increasing interest in these materials, in view of their unique properties.[2] It is possible to synthesize carbon nanoparticles through simple synthetic routes that allow obtaining particles with a variety of properties: different solubility capabilities (water–organic solvent), different sizes and forms, different surface functionalities and tunable optoelectronic properties in the visible region of the electromagnetic spectrum.[2] All of these properties converging in a unique material have generated considerable interest in biomedical, bioanalytical, energy conversion and optoelectronic areas due to its good compatibility with living tissues and potential use in real applications. Along this line, application examples have been reported in photocatalysis,[3] organic light emitting devices,[4] metal ion and gas sensors[5] and bioimaging.[6]

Carbon nanoparticles typically show strong optical absorption in the UV region, with a tail extending out into the visible range and a peculiar light emission behaviour, which has not been observed in other nanoparticles.[2] Also, CNPs are electrochemically active showing electron donor and acceptor capabilities and they are electrochemiluminescent.[2] However, although there are many studies dealing with the physicochemical properties of carbon nanoparticles, the origin of the observed optoelectronic behaviour is even today a topic of discussion.

The origin of the photophysical properties of carbon nanoparticles has been assigned to several reasons in the literature: optical selection of differently sized nanoparticles (quantum effect),[2,3] defects and surface states,[7] surface groups,[6] surface passivation,[2] fluorophores with different degrees of π conjugation,[8,9] recombination of electron–hole pairs localized within small sp^2 carbon clusters embedded within a sp^3 matrix,[10] and free zigzag sites with a carbene-like triplet ground state.[11] More recently, it has been proposed that clusters of few aromatic rings with large enough gaps embedded by the sp^3 carbon matrix are responsible for the optical properties of graphene oxide.[12] Studies performed on graphene ribbon-like systems associated the optical behaviour with edge related phenomena (zigzag and armchair-edge forms, and edge chemical functionalization) and active quantum dots with semiconducting behaviour induced by quantum confinement.[10,14] Keeping in mind the vastness and complexity of the organic chemistry, it is a real challenge to establish the quantum confinement effect on the carbon material properties when they are led to the nanometric scale.

In the present work, a study of hydrophobic carbon nanoparticles obtained by a well-known synthetic procedure,[15] followed by a careful separation method is reported. The purification processes were designed to separate the particles based on their surface chemistry and not by their size or shape,

[a]*Departamento de Química, Universidad Nacional de Río Cuarto, Ruta Nac. 36 - Km. 601, X5804BYA, Río Cuarto, Argentina. E-mail: gmorales@exa.unrc.edu.ar; jfungo@exa.unrc.edu.ar*

[b]*Centro Atómico Bariloche, 8400, S.C. de Bariloche, Argentina*

[c]*Universidad Autónoma de Nuevo León, UANL, CIIDIT, Apodaca, Nuevo León, México*

† Electronic supplementary information (ESI) available: Experimental and characterization details. See DOI: 10.1039/c3nr01485a

producing particles with the fewest number of surface functional groups possible. The relationship between the structure of the carbon nanoparticles and their optoelectronic properties was investigated through an integral study comprising structural characterization, and analysis of electrochemical, photochemical and electrogenerated chemiluminescence behaviour.

2 Experimental section

Carbon nanoparticles were synthesized by modification of the citrate route described by Giannelis.[15,16] The solid dark-brown product obtained after calcination was ultrasonicated in dry tetrahydrofuran (THF) for 30 minutes; then the solids were removed by filtration and washed with THF. The filtrate and washings were combined and vacuum-dried in a rotary evaporator at 45 °C to total dryness (yield 93%). The carbogenic extract was finally separated by column chromatography developed with dichloromethane (see ESI† for full experimental details about the synthesis and characterization of CNPs).

3 Results and discussion

3.1 Transmission electron microscopy

The formation of CNPs was first established by High-Resolution Transmission Electron Microscopy (HRTEM) measurements. Fig. 1 shows representative TEM images where the typical distribution of the carbonaceous nanostructures on the grid can be observed. Examples of agglomerates of the purified carbon particles at low magnification are shown in Fig. 1a and b. Even at such low resolution it is possible to realize that the agglomerates are constituted by objects with different morphologies.

With the purpose of providing a more detailed characterization of the nanoparticles, HRTEM images of individual CNPs were analyzed. Fig. 1c–e present HRTEM images of representative individual CNPs. A general and careful observation allows concluding that the CNPs have a broad distribution in both size and shape, as can be seen in Fig. 1c–e (for more images of representative CNPs see Fig. S1, ESI†). The CNPs have sizes smaller than 50 nm on average and a graphitic structure with variable shapes, *e.g.* polyhedral shells, tubes, horns and onions. Due to the broad dispersion in sizes and shapes, it is difficult to obtain a size distribution from TEM measurements; attempts to obtain it by a bulk technique such as dynamic light scattering failed because of the strong fluorescence emission of the CNP sample.

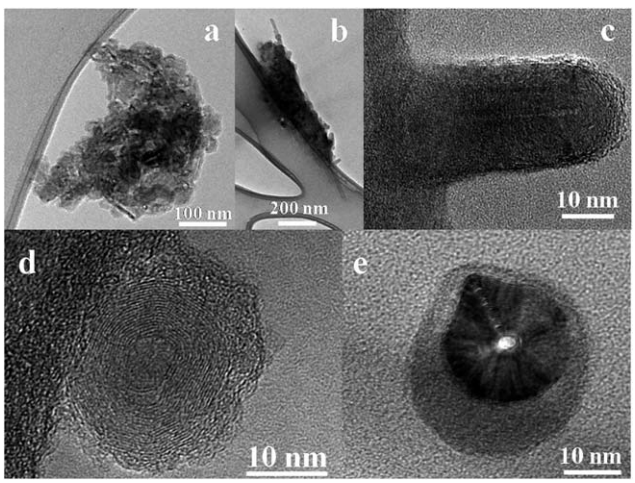

Fig. 1 Representative TEM images of the synthesized CNPs at (a and b) low and (c–e) high-resolution showing different forms and sizes (c and d) and variations within a particular form (d–e).

The observed structures in the TEM images are similar to other carbonaceous materials obtained by other methods.[17–28] High-magnification images revealed that the nanoparticles have a graphitic crystalline core surrounded by an amorphous layer. This is observed in the Fast Fourier Transform (FFT) (see Fig. S2, ESI†) revealing the lack of order within the amorphous shell and the appearance of order in the crystalline core as indicated by the presence of reflections. The core has a graphitic hollow structure, which may present some degree of disorder in the stacking. Its thickness varies even within the same nanoparticle, not being higher than 35 carbon layers. The interlayer spacing is approximately 3.5 Å, which is close to that of the (002) planes of graphite. Variations within each morphology can be found as shown in Fig. 1d–e (and Fig. S1, ESI†), where onion-like particles with an elongated, circular shape or a drop-like shape are observed. The amorphous outer layer approximately mimics the shape of the graphitic component, with a variable local thickness, not being concentric with it, in most cases. These results support the idea of the difference in the type of hybridization presented by the carbon atoms in different regions of the CNPs.

3.2 Spectroscopic characterization

The FTIR spectroscopy was utilized to follow the evolution of the precursor during the thermal treatment and to characterize the purified particles, over the frequency range 4000–700 cm^{-1} (Fig. S3, ESI†). The most important change in the visual appearance and spectrum of the precursor occurs when the temperature of pyrolysis reached 300 °C. There is a significant decrease in the absorbance, which can be attributed to two reasons, the loss of materials or/and a reduction of the IR mass extinction coefficient. The variation in mass of the precursor after the thermal treatment is about 10%, this small difference cannot justify the drop in absorbance observed in the IR spectrum. Besides, the IR mass extinction coefficient of insoluble carbon materials is very sensitive to the internal structure and to small changes in the morphology and agglomeration state of the carbon. Recently, attenuation of the IR mass extinction has been observed for carbonaceous materials produced by laser pyrolysis, which results from the increase of the contents of polycyclic aromatic hydrocarbons, mainly adsorbed on the surfaces of the carbon grains.[29] Then, the decrease in the IR mass extinction coefficient for the sample treated at 300 °C is assigned to the graphitization of the precursor to generate nanoparticles with a graphitic core surrounded by an amorphous layer. The confirmation of the graphitization processes by Raman spectroscopy was unsuccessful because the strong fluorescence emission of the CNP sample masks the expected D and G bands. The FTIR spectrum of the purified nanoparticles

can be described in terms of absorptions from aliphatic carbon chains with some oxygen and nitrogen functionalities, with weak contributions from polyaromatic structures (for a complete description see ESI†).

EELS results confirmed the composition of the CNPs to be of a carbon based material with low content of heteroatom functionalities. The EELS spectrum of the individual CNPs (Fig. S4, ESI†) shows the C–K edge at 284 eV without other visible signals. The N–K edge and the O–K edge are located at 401 eV and 532 eV, respectively; no clear signals of N could be observed in the EELS spectra acquired from different analyzed CNPs although a very small oxygen signal could be present. These results support the idea of the composition of the CNPs being based mostly on carbon, even the amorphous shell layer.

The conventional NMR spectroscopy in liquid media is not useful for the structural characterization of carbonaceous materials because of the sluggish rotation movement of the CNPs in solution and the fast spin–spin relaxation in the rigid structure. Therefore, if a signal is observed, it should be assigned to soluble molecular species and/or functionalities on the surfaces of the nanoparticles.[15,30] The ^{13}C NMR spectrum of the synthesized CNPs in d-chloroform shows signals in the aliphatic region and it is not possible to detect any signals from the sample at chemical shifts higher than ~35 ppm (Fig. S5, ESI†). The NMR studies suggest, on one hand, that aromatic and olefinic soluble molecules are not present in the sample as contaminants. On the other hand, it appears that the purification method allows separating the less oxidized part of the sample.

The above spectroscopic data allow concluding that the purified CNP samples can be described as carbonaceous materials with the carbon atoms in sp^2 and sp^3 states, containing few functional groups mainly derived from oxygen.

3.3 Absorption and photoemission

Fig. 2a shows the light absorption spectrum of CNPs dispersed in THF, where a strong optical absorption is observed in the UV region at 5.29 eV (234 nm), and a shoulder at 4.08 eV (304 nm), with an extending tail to the visible range of the electromagnetic spectrum. When the CNP concentration increases, the shoulder disappears in the extended visible tail, which could indicate some degree of aggregation at a high level of concentration. Fig. 2b shows the steady state normalized emission spectrum of CNPs taken at different excitation wavelengths, where it is clearly noted that the emission maximum is strongly dependent on the excitation wavelength. The energy at the emission maximum moves from 3.01 eV (411 nm) to 2.06 eV (600 nm) as the excitation energy decreases from 5.28 eV (235 nm) to 2.16 eV (575 nm) producing a red shift of 0.95 eV (189 nm). On the other hand, an emission quantum yield value of 12% was measured at 355 nm excitation in THF (for calculation details see ESI†). This value of emission quantum yield is in the range of other carbonaceous nanoparticles reported in the literature.[7,9,31]

Fig. 3a shows the energy values of the luminescence peak maximum and its corresponding emission intensity obtained from Fig. 2b as a function of the excitation beam energy. Both the

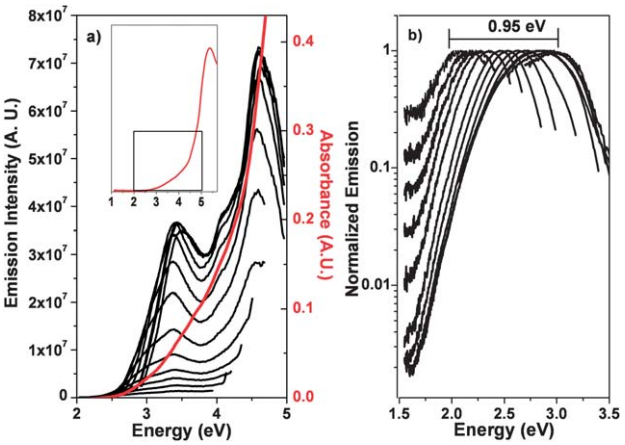

Fig. 2 (a) Light absorption spectrum (red line) and photoluminescence excitation spectra measured at the emission maximum values shown in Fig. 3b (black lines). Inset: CNP light absorption spectrum in the range from 1.5 eV (210 nm) to 5.9 eV (800 nm). (b) Normalized fluorescence spectra of CNPs dispersed in THF taken by increasing progressively the excitation wavelengths from 3.1 eV (400 nm) to 2.1 eV (575 nm) every 25 nm.

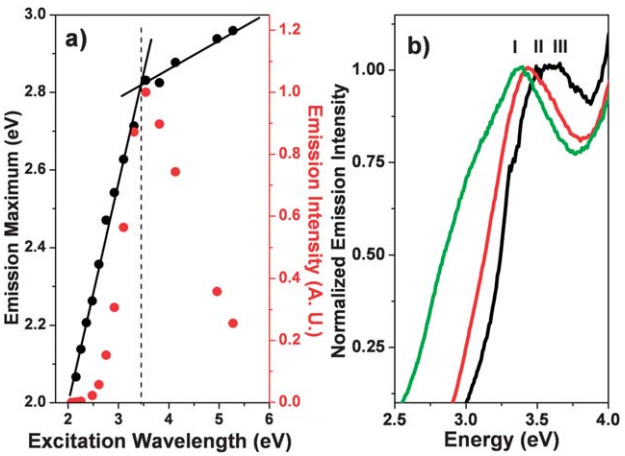

Fig. 3 (a) Energy values of the luminescence peak maximum and its corresponding emission intensity obtained from Fig. 2b *versus* the excitation beam energy. (b) Normalized photoluminescence excitation spectra measured at I: 2.94 eV (422 nm), II: 2.80 eV (442 nm), and III: 2.19 eV (567 nm).

emission intensity and the emission energy maximum have an abrupt change in their tendency after the dispersion of CNPs is excited at 3.46 eV (358 nm), which indicates that different photochemical mechanisms are operative. The optical behaviour suggests that the fluorescence of CNPs is composed of a dual emission, which is in agreement with the recent observations made in temperature-dependent experiments. Yu *et al.* proposed that the dual light photoemission of carbon dots is due to the presence of both the carbogenic core and the surface molecular fluorophores.[32] Then, an energy value of 3.46 eV, where the change in the tendency of the emission maximum matches with the maximum of the emission intensity (see the dotted line in Fig. 3a), can be associated with a main operative state or with a band gap. While the states below 3.46 eV can be assigned to the surface states. In addition, it is observed that the fluorescent full width at half maximum (FWHM) also depends on the excitation

energy. The FWHM continually decreases from 0.82 eV (130 nm) to 0.42 eV (89 nm) when the CNPs are excited in the range of 3.8 eV (325 nm) to 2.75 eV (450 nm) respectively. This could indicate that the emission with a narrower FWHM at low energy can be associated with isolated sp^2 domains (or traps).[32,33]

The optical behaviour of CNPs (Fig. 2) is similar to that observed in other studies of carbon nanoparticles reported in the literature.[2] The optical characteristics of CNPs have been attributed to different mechanisms. H. Zhen *et al.* reported that reduced carbon nanoparticles emit light with a maximum in the blue region, while more oxidized particles emit in the green-red region of the electromagnetic spectrum.[31] Therefore, the observed CNP emission maximum at 3.46 eV (358 nm) (see Fig. 3a) indicates that the CNPs are in a reduced state, with a less number of oxidized oxygen-functional groups, in agreement with the results obtained by FTIR and EELS characterization.

Otherwise, the TEM studies show that the synthesized CNPs are heterogeneous in size and shape. Therefore, a possible explanation for the observed optical behaviour is associated with the selective optical absorption and emission of nanoparticles with different sizes and forms. However, this interpretation is not supported by previous studies in this area. For example, there are reports on CNPs with different sizes (from ~1 to 60 nm), such as monodisperse carbon dots,[34] particles with narrow and wide diameter distributions,[9,14,35] forms and morphologies such as spheres,[10,15] discs,[10] and onions,[21] diverse chemical functionalities and characteristic of the surface (*e.g.* hydrophilic, hydrophobic, functionalized, unfunctionalized)[36] and all of them in general show an optical behaviour similar to the one observed in Fig. 2a and b. Therefore, it is reasonable to propose that at least for the CNPs synthesized in this work, the carbon nanoparticles have a common feature, which is independent of their form, size and surface chemistry, that rules their optoelectronic properties.

The structure of the amorphous carbon is poorly defined and until now, the Robertson's model has been the most referred and successful.[37] According to this model, the material consists of sp^2 clusters embedded in the sp^3 bonded matrix. The optoelectronic properties of the amorphous carbon materials have been studied for a long time. One of the interesting features of amorphous carbon is its capability to exhibit strong photoluminescence emission at room temperature. Reported studies showed that amorphous carbon films under determinate conditions have similar luminescence behaviour to that observed for the CNPs in this work (see Fig. 2).[38,39] The photoluminescence of amorphous carbon materials takes place at the spatially confined π–π^* states, which generate localized electron–hole pairs under excitation. The variation of cluster sizes and local environment, where the excited states are localized, produces changes in the efficiency and emission energy of the recombination processes for the electron–hole pair. For large clusters, the π–π^* states are delocalized and the non-radiative recombination of the electron–hole pairs is dominant, while in small clusters the radiative recombination occurs.[38–41] For optical transitions inside of the cluster containing sp^2 carbon atoms, the electron–hole pair confinement manifests as a resonance effect that can be detected in the photoluminescence excitation spectrum. It has been estimated that luminescence clusters, which allow the localization and radiative recombination of the electron–hole pairs, have a size of approximately one nm.[38,39,41]

The excitation spectra in Fig. 2a display two well-defined peaks, one at ~4.6 eV (270 nm) with a shoulder at 4.05 eV (306 nm), and the other at ~3.44 eV (360 nm), indicating that there are some states with larger emission capability than others. On the other hand, it is observed that the position of the peak at 4.6 eV (270 nm) is not sensitive to the emission energy, while the position of the lower energy peak changes noticeably with the emission energy (see Fig. 2a and 3b). This particular optical behaviour of the CNPs has been previously observed in amorphous carbon films.[38–41] Keeping in mind that the synthesized CNPs are formed from a crystalline core covered by an amorphous carbon shell, it is reasonable to propose that the amorphous shell, which is present in all the CNPs independent of their size and shape, plays an important role in the photoemission behaviour or mechanism. The luminescence model for amorphous carbon materials postulates that the photoexcitation takes place inside the sp^2 domain or clusters, which behave as luminescence centres where the spatial confinement of electron–hole pairs takes place.[38–41] In general, in the CNPs three regions can be observed, the core formed by crystalline sp^2 structures, a carbon amorphous shell and surface groups. The existence of two identifiable photophysical active centres in the excitation spectra (see Fig. 2a) implies that there are two kinds of sp^2 clusters.[32] In one group, the sp^2 clusters are isolated from each other and are not sensitive to the emission energy. They can be identified with the crystalline core or more likely with the molecular polyaromatic species isolated into the sp^3 carbon matrix of the amorphous shell. The second group is formed by a distribution of sp^2 clusters close enough to allow interaction between them. The interacting clusters together with the surface functional groups (minimized in this work) can produce photostimulated charge and energy transfer defining the main optical characteristic of CNPs observed in the visible region of the electromagnetic spectrum. This highlights the role of the amorphous shell in CNP optical properties and improves the previously proposed model for carbon nanoparticles, where the dual fluorescence behaviour was attributed to the emission from the core and the surface states.[32]

3.4 Electrochemistry

The electrochemistry of CNPs was studied to obtain information about the electronic structure, band gap and band edge, charge transfer process at the electrode interface and stability of charged nanoparticles.

The cyclic voltammograms of the CNPs displayed poorly defined waves corresponding to diffusion controlled electrochemically reversible processes (see Fig. S6, ESI†). This observation allows discarding adsorption of electroactive materials on the electrode surface. The DPV of the same dispersion (Fig. 4a) showed five successive reduction and complementary oxidation waves with a typical shape of reversible processes involving stable negatively charged species at −1.43 V, −1.65 V, −1.95 V, −2.12 V and −2.61 V.

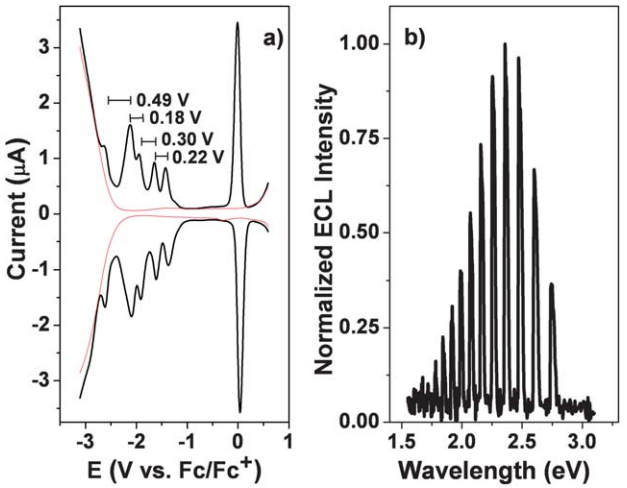

Fig. 4 (a) DPV of CNPs dispersed in THF (0.1 mol L^{-1} $TBAPF_6$). The red curve is the DPV of the solution free of CNPs. (b) CNP spectrum of ECL emission at the Pt electrode in THF containing 10 mM of BPO, obtained by cyclic square wave excitation at 0.2 Hz between 0 and 2.8 V *vs.* Fc/Fc^+.

Nowadays a few electrochemical studies have been reported for CNPs, carbon nanodiamonds and carbon onions;[30,42,43] and the origin of the redox properties observed is a matter of study.[2] In general, CNPs can show the four possible electrochemical behaviours described for metallic nanoparticles in the literature:[44] bulk-continuum, quantized double-layer charging, molecule-like and also, the signal ruled by redox active groups present on the CNP surface such as quinones, lactones, ethers, epoxides, esters, aliphatic amines, amides, among others. Besides, it has been reported that CNPs can serve as excellent electron donors and strong electron acceptors.[2,42,43,45] In spite of the numerous studies reporting the synthesis of CNPs using electrochemical methods,[44,46,48] there are only a few studies addressing their redox properties.[30,42]

A careful observation of the DPV signal permits determination of the nature of the nanoparticle core charging process. The DPV of CNPs (Fig. 4a) shows a region between the first reduction process and the anodic limit of the solvent where no voltammetric features are observable. Therefore, the mentioned voltammetric characteristics exclude the possibility of associating the electrochemical behaviour of CNPs with: (i) a bulk continuum (voltammetric features are observed, Fig. 4a) and (ii) a quantized double layer charging effect (an energy gap is observed, Fig. 4a).[44] The region in the DPV of the nanoparticles where no voltammetric features are observable could indicate the presence of a band gap, which is a typical electrochemical behaviour of molecule-like nanoparticles.[44] Thus, the first reduction processes (−1.42 V) can be assigned to the position of the lowest unoccupied molecular orbital (LUMO).[46] Then, from the optical gap (~3.5 eV), it is possible to estimate the energy position of the highest occupied molecular orbital (HOMO). The HOMO potential was estimated at ~2.08 V *vs.* Fc/Fc^+, a value that is out of the electrochemical window for the solvent/electrolyte where the nanoparticles are soluble. The experimental impossibility to study the oxidation process for CNPs does not allow determining a value of the electrochemical band gap and further comparison with the optical band gap. Although the functional groups have been minimized by the purification procedure, remaining electroactive redox groups or traps on the surface of the CNPs cannot be completely discarded. However, Fig. 4a shows a pattern in the electrochemical peaks where two separated doublets can be observed. This regularly spaced current peak is characteristic of consecutive single electron transfer events, which can be associated with well-defined molecular orbitals, in agreement with a typical electrochemistry of molecule-like nanoparticles.[44]

It has been established that the electrochemical behaviour of nanoparticles is strongly dependent on their size and polydispersity.[44] To prove this, monodisperse metal nanoparticles with different sizes have been studied. Only small and highly monodisperse nanoparticles exhibit well-solved and regularly spaced redox waves, including a central gap. However, the characterizations showed that the CNPs synthesized in this work (see Fig. 1) are a mixture of a wide range of sizes and shapes excluding soluble conjugated molecular species as impurities. Therefore, the observed electrochemical behaviour of CNPs cannot be interpreted as a function of sizes and geometric forms. Instead, the electrochemical response could originate from a molecular structure present in all CNPs independent of their size and shape. The common structure present in all the CNPs is the outer amorphous layer surrounding the fullerene-like multishell nanoparticle core. In agreement with the conclusions reached in the photophysical section, the electrochemical studies suggest that the structure and chemical composition of the amorphous carbon shell are very important to determine the optical and electrical properties of CNPs. It should be noted that, at least for the CNPs reported in this work, the origin of "molecular like behaviour" could not be associated with a particle size-related quantum confinement effect. Probably the size, chemical composition and spatial distribution of sp^2 domains within the amorphous outer shell control the observed behaviour. A similar model has been proposed for graphene derivative materials where it is suggested that the optoelectronic properties are originated from the sp^2 fragments embedded in a saturated carbon two dimensional matrix (with LUMO–HOMO gaps within 0.9–5.8 eV) and the edge effect of polyaromatic rings.[13]

3.5 Electrogenerated chemiluminescence

The ECL is a useful tool for the analysis of optoelectronic characteristics, because it allows correlating the CNP electrochemical and optical properties with the molecular structure. The ECL is a process whereby species generated at electrodes undergo high-energy electron transfer reactions to form excited states that emit light. As it was mentioned in the electrochemical analysis, the HOMO potential of CNPs was estimated at ~2.08 V *vs.* Fc/Fc^+, a value that is out of the electrochemical window for the solvent/electrolyte where the CNPs are soluble. Consequently, for CNPs, a cathodic coreactant must be used to study the ECL properties. There are not many cathodic coreactants soluble in THF, for this system, BPO was selected as the coreactant.[49] The ECL spectrum for the CNPs obtained in the presence of BPO is shown in Fig. 4b. No ECL emission was

observed in the dispersion containing CNPs without BPO, which indicates that the annihilation process between the negatively charged particles and the oxidizing BPO radicals is an ECL operative process. The ECL capability of the material is in agreement with previous reports for similar systems.[42,46,50] Until now only a few examples of cathodic ECL have been observed.[46] In order to obtain detectable light intensity, it was necessary to apply a larger potential than the second CNP redox processes, suggesting that the first two negatively charged states of CNPs are not ECL active. Taking into account that for CNPs the first reduction occurs at −1.42 V and the redox potential value for the couple $C_6H_5CO_2^{\cdot}/C_6H_5CO_2^{-}$ is larger than +1.5 V *vs.* SCE,[49] the energy of the annihilation reaction between these species is not enough to excite CNP particles with a 3.5 eV band gap. In Fig. 4b is observed a maximum energy value of ECL emission at 2.35 eV, which is 0.50 eV red-shifted compared with the photoluminescence maximum shown in Fig. 3. This redshift cannot be only associated with the insufficient energy from the annihilation reaction between the BPO and CNPs. This fact can also be assigned to a space distribution of the emission states in the particle. Due to the nature of the ECL mechanism, it is expected that the annihilation reaction between the coreactant and negatively charged CNPs occurs on the particle surface. The results suggest that the emission observed in the ECL spectrum originates from the surface of the amorphous carbon shell, where there are accessible sp^2 domains and functional groups; while the photoluminescence spectrum shows the emission produced by the excitation of surface and bulk of the particle.

4 Conclusions

In summary, a synthetic procedure and a purification method are reported which yield carbon nanoparticles that are insoluble in water with a small number of surface functional groups. The CNPs are polydisperse in size and shape. Based on the evidence of change of the carbon atom hybridization in different regions of individual nanoparticles, it was concluded that they have a structure composed by a fullerene-like multishell surrounded by an amorphous carbon layer. The nature of the electro-optic properties was studied and correlated with the morphological and chemical characteristics of the material. For the synthesized nanoparticles, the results showed that the optoelectronic behaviour could not be associated with nanoparticle size and shape-related quantum confinement effects. Instead, the synthesized CNPs have an outer amorphous layer, the properties of which are independent of their particle form and size. The mentioned outer amorphous layer may play an important role in determining the optoelectronic properties of the nanoparticles. Future work focused on the amorphous outer shell of CNPs will help to answer remaining open questions in the field.

Acknowledgements

We thank CONICET, ANPCyT and UNRC for financial support. The authors also thank the ICNAM at the University of Texas at San Antonio for the support provided for the use of their Advanced Microscopy Center. GMM, MSM and FF are scientific members of CONICET.

Notes and references

1 X. Xu, R. Ray, Y. Gu, H. J. Ploehn, L. Gearheart, K. Raker and W. A. Scrivens, *J. Am. Chem. Soc.*, 2004, **126**, 12736.
2 S. N. Baker and G. A. Baker, *Angew. Chem., Int. Ed.*, 2010, **49**, 6726.
3 H. Li, X. He, Z. Kang, H. Huang, Y. Liu, J. Liu, S. Lian, C. H. A. Tsang, X. Yang, S.-T. Lee and S.-T. Lee, *Angew. Chem., Int. Ed.*, 2010, **49**, 4430.
4 F. Wang, Y.-H. Chen, C.-Y. Liu and D.-G. Ma, *Chem. Commun.*, 2011, **47**, 3502.
5 W. Wei, C. Xu, J. Ren, B. Xu and X. Qu, *Chem. Commun.*, 2012, **48**, 1284.
6 Y. Fang, S. Guo, D. Li, C. Zhu, W. Ren, S. Dong and E. Wang, *ACS Nano*, 2012, **6**, 400.
7 S.-L. Hu, K.-Y. Niu, J. Sun, J. Yang, N.-Q. Zhao and X.-W. Du, *J. Mater. Chem.*, 2009, **19**, 484.
8 X.-J. Mao, H.-Z. Zheng, Y.-J. Long, J. Du, J.-Y. Hao, L.-L. Wang and D.-B. Zhou, *Spectrochim. Acta, Part A*, 2010, **75**, 553.
9 A. B. Bourlinos, R. Zbořil, J. Petr, A. Bakandritsos, M. Krysmann and E. P. Giannelis, *Chem. Mater.*, 2012, **24**, 6.
10 S. Srivastava and N. S. Gajbhiye, *ChemPhysChem*, 2011, **12**, 2624.
11 D. Pan, J. Zhang, Z. Li and M. Wu, *Adv. Mater.*, 2010, **22**, 734.
12 D. Pan, J. Zhang, Z. Li, C. Wu, X. Yan and M. Wu, *Chem. Commun.*, 2010, **46**, 3681.
13 G. Eda, Y. Lin, C. Mattevi, H. Yamaguchi, H. A. Chen, I. S. Chen, C. W. Chen and M. Chhowalla, *Adv. Mater.*, 2010, **22**, 505.
14 R. Liu, D. Wu, X. Feng and K. Müllen, *J. Am. Chem. Soc.*, 2011, **133**, 15221.
15 A. B. Bourlinos, A. Stassinopoulos, D. Anglos, R. Zboril, M. Karakassides and E. P. Giannelis, *Small*, 2008, **4**, 455.
16 M. J. Krysmann, A. Kelarakis, P. Dallas and E. P. Giannelis, *J. Am. Chem. Soc.*, 2012, **134**, 747.
17 N. Sano, H. Wang, M. Chhowalla, I. Alexandrou and G. A. J. Amaratunga, *Nature*, 2001, **414**, 506.
18 X. H. Chen, H. S. Yang, G. T. Wu, M. Wang, F. M. Deng, X. B. Zhang, J. C. Peng and W. Z. Li, *J. Cryst. Growth*, 2000, **218**, 57.
19 V. L. Kuznetsov, A. L. Chuvilin, Y. V. Butenko, I. Yu. Malkov and V. M. Titov, *Chem. Phys. Lett.*, 1994, **222**, 343.
20 S. Hu, J. Yang, W. Liu, Y. Dong and S. Cao, *Carbon*, 2011, **49**, 1505.
21 X. Li, H. Wang, Y. Shimizu, A. Pyatenko, K. Kawaguchi and N. Koshizaki, *Chem. Commun.*, 2011, **47**, 932.
22 V. Z. Mordkovich, *Chem. Mater.*, 2000, **12**, 2813.
23 M. Choi, I. S. Altman, Y.-J. Kim, P. V. Pikhitsa, S. Lee, G.-S. Park, T. Jeong and J.-B. Yoo, *Adv. Mater.*, 2004, **16**, 1721.
24 R. L. Vander Wal and M. Y. Choi, *Carbon*, 1999, **37**, 231.
25 T. Gorelik, S. Urban, F. Falk, U. Kaiser and U. Glatzel, *Chem. Phys. Lett.*, 2003, **373**, 642.
26 A.-B. Du, X.-G. Liu, D.-J. Fu, P.-D. Han and B.-S. Xu, *Fuel*, 2007, **86**, 294.

27 R. L. Vander Wal, A. J. Tomasek and T. M. Ticich, *Nano Lett.*, 2003, **3**, 223.
28 W. A. De Heer and D. Ugarte, *Chem. Phys. Lett.*, 1993, **207**, 480.
29 C. Jäger, F. Huisken, H. Mutschke, T. Henning, W. Poppitz and I. Voicu, *Carbon*, 2007, **45**, 2981.
30 L. Tian, D. Ghosh, W. Chen, S. Pradhan, X. Chang and S. Chen, *Chem. Mater.*, 2009, **21**, 2803.
31 H. Zheng, Q. Wang, Y. Long, H. Zhang, X. Huang and R. Zhu, *Chem. Commun.*, 2011, **47**, 10650.
32 P. Yu, X. Wen, Y.-R. Toh and J. Tang, *J. Phys. Chem. C*, 2012, **116**, 25552.
33 C.-T. Chien, S.-S. Li, W.-J. Lai, Y.-C. Yeh, H.-A. Chen, I.-S. Chen, L.-C. Chen, K.-H. Chen, T. Nemoto, S. Isoda, M. Chen, T. Fujita, G. Eda, H. Yamaguchi, M. Chhowalla and C.-W. Chen, *Angew. Chem., Int. Ed.*, 2012, **51**, 6662.
34 B. Zhang, C.-Y. Liu and Y. Liu, *Eur. J. Inorg. Chem.*, 2010, **2010**, 4411.
35 S. Hu, Y. Guo, W. Liu, P. Bai, J. Sun and S. Cao, *J. Phys. Chem. Solids*, 2011, **72**, 749.
36 H. Peng and J. Travas-Sejdic, *Chem. Mater.*, 2009, **21**, 5563.
37 J. Robertson, *Mater. Sci. Eng., R*, 2002, **37**, 129.
38 M. Fule, M. Budai, J. Toth, S. Veres and M. Koós, *J. Non-Cryst. Solids*, 2006, **352**, 1340.
39 M. Fule, S. Tóth, M. Veres, I. Pócsik and M. Koós, *Diamond Relat. Mater.*, 2005, **14**, 1041.
40 F. Demichelis, S. Schneiter and A. Tagliaferro, *Phys. Rev. B*, 1995, **51**, 2143.
41 T. Heitz, C. Godet, J. E. Bouree, B. Drevillon and J. P. Conde, *Phys. Rev. B*, 1999, **60**, 6045.
42 J. Zhou, C. Booker, R. Li, X. Zhou, T.-K. Sham, X. Sun and Z. Ding, *J. Am. Chem. Soc.*, 2007, **129**, 744.
43 J. Zhou, C. Booker, R. Li, X. Sun, T.-K. Sham and Z. Ding, *Chem. Phys. Lett.*, 2010, **493**, 296.
44 R. W. Murray, *Chem. Rev.*, 2008, **108**, 2688.
45 X. Wang, L. Cao, F. Lu, M. J. Meziani, H. Li, G. Qi, B. Zhou, B. A. Harruff, F. Kermarrec and Y.-P. Sun, *Chem. Commun.*, 2009, **25**, 3774.
46 Q.-L. Zhao, Z.-L. Zhang, B.-H. Huang, J. Peng, M. Zhang and D.-W. Pang, *Chem. Commun.*, 2008, **41**, 5116.
47 J. Lu, J.-X. Yang, J. Wang, A. Lim, S. Wang and K. P. Loh, *ACS Nano*, 2009, **3**, 2367.
48 L. Zheng, Y. Chi, Y. Dong, J. Lin and B. Wang, *J. Am. Chem. Soc.*, 2009, **131**, 4564.
49 A. J. Bard, *Electrogenerated Chemiluminescence*, Marcel Dekker, New York, 2004.
50 F.-R. F. Fan, S. Park, Y. Zhu, R. S. Ruoff and A. J. Bard, *J. Am. Chem. Soc.*, 2009, **131**, 937.